

Thermo-opto-electrical characterization of Photovoltaic Devices: Performance and Longevity

R. Dix-Peek*, R. Roodt, E.E. van Dyk, J Crozier McClelland, M. Vumbugwa, F. Vorster

Ross.Dix-Peek@mandela.ac.za*

Nelson Mandela University

Abstract

There are many different ways to assess the performance of a Photovoltaic (PV) module; whether through electrical measurements such as dark and/or light current-voltage measurements or imaging-based techniques such as thermography (IR imaging, dark lock-in thermography, etc) and luminescence imaging (photoluminescence or electroluminescence imaging). All of these techniques can provide some information regarding the performance of the PV device; however, the application of more than a single technique can provide a more complete analysis and interpretation. PV modules often contain defects, some of which are material defects, manufacturing defects and some even handling and installation defects. The defects are often performance limiting and can over time become more pronounced, the module performance then degrades with time. However, operational failures can play a more destructive role. This paper investigates the application of these techniques at the PV cell scale and at the PV module scale to find a plausible explanation for a particular operational failure.

Keywords: Photovoltaic, luminescence imaging, thermography

1. Introduction

As many countries across the world have begun moving towards their Decarbonisation targets, Renewable Energy technologies have become increasingly popular. One such technology is solar PV. The cumulative capacity installed globally is believed to have hit the ~1010 GW mark as of 2022 (PV Magazine, 2022) and in South Africa it is 4172 MW (ESI Africa, 2021). Considering this increase in PV technology market penetration, quality control measures become important to ensure the protection of the end user. PV system and module level thermo-optoelectrical characterisation is already used in the quality control of PV module manufacturing and PV system operation and maintenance (Haney, J., and Burstein, A., 2013). Thermo-opto-electrical characterisation can also be used to test newer PV cell technologies' performance and longevity in real world applications (Bauer, J., Breitenstein, O. and Wagner, J., 2009; Fuyuki, T., et al, 2005; Wurfel, P., 2005). This paper looks at specific operational failures and features noted in PV systems and deployed modules and investigates the cell-level defects that are likely responsible. On the module string and module level, thermography, Electroluminescence (EL) imaging and electrical measurements were used to investigate the operational mismatch of PV cells within a module. On the cell level, dark lock-in thermography is used to investigate the effects of individual cell reverse bias and highlight the locality of the resultant hotspots. This multi-probe investigation gives insight into the operation of defective cells within a PV module.

In-field operation will often result in PV modules operating outside of ideal operating conditions. The resultant thermal images will then vary depending on those operating conditions and the hotspots that can form when the cells within a module operate at conditions that can cause them to begin to dissipate heat. As shown in this paper, a simple electrical mismatch can cause individual cells to become reverse biased. Similarly, the shading of cells can cause short circuit current mismatch between the cells, forcing the shaded cell to operate in a reverse bias state where the current matches that of the module. This is typically minimised by the use of bypass diodes which limit the

reverse bias voltage by the number of cells within the cell substring within the PV module. This results in a reverse bias voltage potential of approximately 12~16 V depending on the length of the cell string. However, if the bypass diode is not present or is not functioning appropriately, the potential reverse bias is limited to that of the entire module string in operation. Depending on the electrical characteristics of the reverse biased cell and the level of shading, the heat dissipation through the area of an individual cell can get as high as ~200 W. Figure 1 is an image of a burnt back sheet of a module that likely had a reverse biased cell over an extended period of time. The locality of the burning is indicative of this.



Figure 1 Burnt back sheet of crystalline Silicon PV module.

For the sake of brevity, a brief description of the techniques applied is included in this section. However, a more detailed description of the techniques is included in the references used in the corresponding subsections.

1.1. Standard thermography

Standard IR thermography of PV modules includes both dark thermography (DT) and Thermal Infrared imaging (TIR). DT has the requirement of the module/device not being in operation and therefore needing electrical input to induce temperature variation within the module/device. This has the benefit of control of input and can be used to detect localised shunting, electrical shorts and disconnections. TIR is the thermal imaging of PV modules in operation, where localised hotspots can be detected (Buerhop, C., et al., 2016; Dotenco, S., et al., 2016). It is also a cost and -time-effective technique as it can be done under standard operational conditions. However, variation in module operation conditions can affect the resultant TIR image and interpretation (Vumbugwa, M., et al, 2022).

1.2. Dark Lock-in thermography

One of the major drawbacks of dark thermography is that due to the high thermal conductivity of Silicon used for PV cells. Localised device heating is blurred, limiting the ability to determine the local power dissipation density (decrease in spatial resolution). By pulsing the power source, being light or electrical stimulation, it is possible to increase the spatial resolution through lock-in thermography (Bauer, J., Breitenstein, O. and Wagner, J., 2009). Dark Lock-in Thermography (DLIT) is more specifically electrically stimulated lock-in thermography. Figure 2 is the graphical representation of the lock-in procedure and the applied weightings for each thermal image per lock-in period. The duty cycle of the electrical stimulus is dependent on the application; however, as shown in the figure, the typical duty cycle is 50%. The thermal camera is triggered at a frequency of a minimum twice that of the frequency applied to the device under test. Equation 1 shows how the in-phase image (T^0) is calculated, while Equation 2 shows how the out-phase image (T^{-90}) is calculated. The resultant images have a much greater spatial resolution than a single dark thermal image. The amplitude image (A), which considers both the in-phase and out-phase image, is calculated using Equation 3. Local power density is usually calculated using this amplitude image as it gives an indication of local current density.

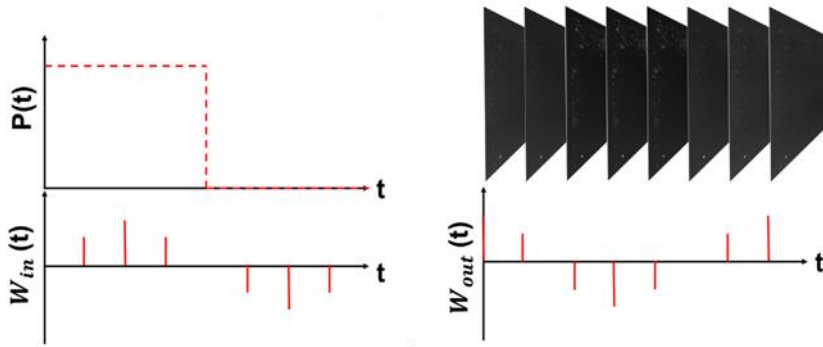


Figure 2 Graphical Representation of DLIT imaging process and the applied weightings for each thermal image.

$$T^0 = \frac{1}{Nn} \sum_{k=1}^N \sum_{m=1}^n 2 * F_{k,m} * \sin\left(\frac{2\pi(m-1)}{n}\right) \dots\dots\dots(1)$$

$$T^{-90} = \frac{1}{Nn} \sum_{k=1}^N \sum_{m=1}^n (-2) * F_{k,m} * \cos\left(\frac{2\pi(m-1)}{n}\right) \dots\dots\dots(2)$$

$$A = \sqrt{(T^0)^2 + (T^{-90})^2} \dots\dots\dots(3)$$

Where N is the number of periods the device is powered (power pulse signals), n is the number of thermal images taken per pulse period, F is the thermal image taken during the image acquisition pulse.

1.3. Electroluminescence

Light emitting diodes (LEDs) are well-known devices in the modern world, PV cells can be seen as a spatially distributed near-infrared LED device (Rau, U., 2007). Under an electrical stimulus, light is generated by a PV cell under a process named electroluminescence (if the light is induced the luminescence is termed photoluminescence). This can then be imaged using a sensor that has the appropriate wavelength sensitivity. The local intensity of light detected by each pixel is dependent on the optical, electrical characteristics and local junction voltage of the device under test. The relationship between measured luminescence signal and local junction voltage is described in Equation 4 (Fuyuki, T., and Kitiyanan, A., 2008; Dix-Peek, R.M., van Dyk and E.E., Vorster, F.J., 2021).

$$\phi^{x,y}(V) = C^{x,y} \exp\left(\frac{V^{x,y}}{kT^{x,y}}\right) \dots\dots\dots(4)$$

Where $\phi^{x,y}$ is the locally detected luminescence, $C^{x,y}$ is the local calibration constant dependent on local device and system properties, k is the Boltzmann constant in eV/K units, $V^{x,y}$ is the local junction voltage, $T^{x,y}$ is the absolute local junction temperature.

2. Experimental Procedure

2.1. Module level experimentation

A polycrystalline module was modified for the experimental work included in this study. Sections of the back sheet and encapsulant were removed, allowing for electrical contact to be made with the individual cells of this module. These contacts were used to measure the voltages of each cell while the module was in operation. The exact details of this experimental setup are included in the work by Vumbugwa, et al. (Vumbugwa, M., et al, 2022). The module was placed onto a north-facing stand, with an inclination of 34° under solar irradiance between 700-1000 W/m². The load was varied, changing the operational conditions of the module, the details are summarised in Table 1. Thermal images were taken of the module during the same periods as the voltage measurements.

Table 1. Experimental operation conditions of Si PV module under test.

Current (A)	Voltage (V)	Period (s)
1.48	33.5	0-165
6.89	27.0	166-480
7.80	24.0	481-805
7.81	18.0	806-1220
7.77	0.2	1221-1630

2.2. Cell level experimentation

A 6-inch polycrystalline PV cell was selected to undergo EL imaging and forward and reverse bias DLIT. While the PV cell is not precisely the same as those found in the previously tested module, the base technology is very similar and therefore, the thermo-opto-electrical characteristics are similar.

The EL experimental setup made use of a KEPCO BOP 36-12M-802E power supply in constant current mode. Two Agilent 34410A digital multimeters were used to measure both applied voltage and current. The camera used to image the EL signal from the Si cell was a Basler acA2040-90um NIR, which is an extended NIR Si-based sensor.

The DLIT setup made use of the same power supply as the EL setup; however, the thermal camera was used to trigger the power supply. The pre-built DLIT software controlled the frequency of both the camera and the power supply.

3. Results

3.1. Module level results

The PV module used in this work consists of 60 series connected Si PV cells. As they are in series, each of the module's substring currents is equal to the cell current within that substring. Therefore, any variation in electrical characteristics or short circuit current causes a variation in operation point for the cells. The results shown in this subsection are from a manuscript in preparation and thesis (Vumbugwa, M., 2022). Figure 3 (a) is the TIR image of the PV module at the operational condition 1.48 A and 33.5 V, while (b) is the TIR at 6.89 A and 27.0 V, (c) is the TIR at 7.80 A and 24.0 V, (d) is the TIR image at 7.81 A and 18.0 V, and (e) is the TIR image at 7.77 A and 0.2 V. In Figure 3 (f), the decreased current from module operation voltage 18.0 V to 0.2 V is likely due to changing environmental conditions or the effect of localised heating as seen in the thermal image. Figure 3 (f) is measured voltages of the individual cells of the module. Figure 3 (a) and (b) show very little variation in the temperature across the module and that corresponds with the minimal variation in operation conditions (the same current and similar voltages). However, as the operational current of the module moves to short circuit conditions, the cell voltage variations increase which corresponds to an increase in variation in the TIR of the module.

The cell numbering is given in Figure 3 (e), with the cells of interest given indicated by a block and number. Looking at cell 1, highlighted in Figure 3 (e), the temperature of the cell does not increase significantly from near open circuit to short circuit condition. This can be attributed to the fact that the cell does not get reverse biased (as seen in Figure 3 (f)). Looking at cell 8, the cell temperature only begins increasing after the module voltage is 18V or lower. At that point, the cell voltage begins to become negative (in Figure 3 (f) the cell operates near 0V at this point oscillating between positive bias and negative bias). However, cell 34 shows an increased temperature from 24 V, this corresponds with a reverse biasing of the cell as seen in (f). Another interesting feature noted in (f) is the fact that there exists a spectrum of cell voltages within the module between -1.5 V and 0.36 V. This is evidence that even under operational conditions where the module is not shaded, or does not contain cells that are partially isolated, the variation in cell electrical characteristics can cause the cell to become reverse biased. If a cell was partially isolated or shaded, the effect could be significantly worse.

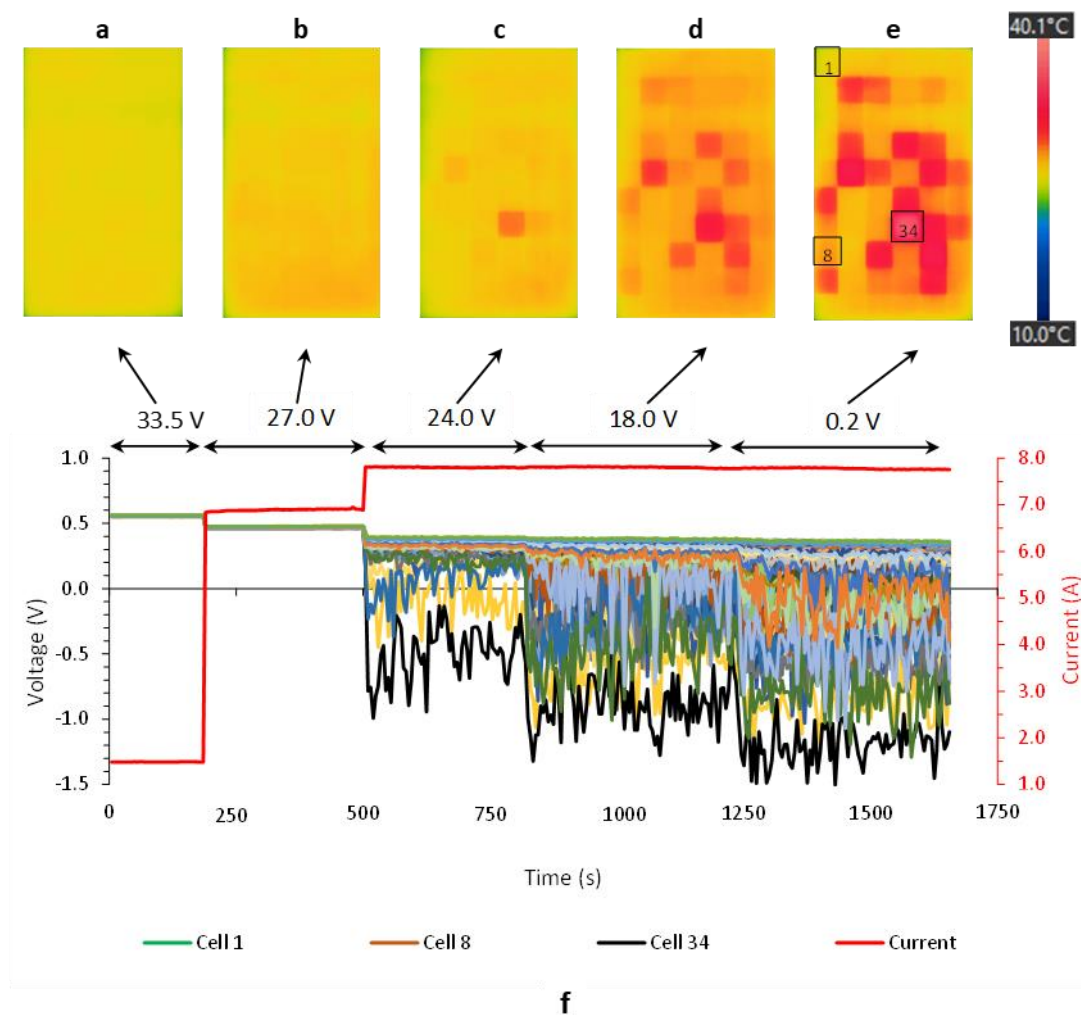


Figure 3 Module current, cell voltages and thermal characteristics of a polycrystalline PV module recorded under different operational voltages.

3.2. Cell level results

As discussed, and shown in the introduction, in-field operation can cause severe localised heating in a PV module. Figure 4 (a) is the EL image of the multi-crystalline Si PV cell under test at 0.7 V and 10 A, (b) is the forward bias DLIT image at 0.7 V and 10 A, (c) is the DLIT image at -18 V and -2 A, and (d) is the DLIT image at -22 V and -8 A. In the EL image of the cell microcracks can be seen emanating from the busbars, likely formed in the soldering process (one being indicated by A). The increased contrast from left to right of the cell was likely a result of non-ideal soldering (the image

gets significantly darker moving away from the busbars). The variation in contrast is likely due to increased series resistance decreasing the local junction voltage relative to the voltage applied to the cell. Dark regions (such as the one indicated by B) are related to defects within the grain boundaries within the multi-crystalline material. These defects act as either alternative current paths or allow for defects that allow for increased carrier recombination at the defects. In (b), (c), and (d) the microcrack noted by A is visible and associated with an increase in power density. This is indicative of localised shunting, or weak non-linear recombination (Breitenstein, O., et al, 2004). While this crack does show localised heating it is not significant. Feature B, which appeared dark in (a) shows increased power density in (b) and (d) relative to unaffected regions. This implies that even while under high forward bias condition, (b), the local current density is higher than the surrounding material. That is, defect-related recombination is occurring in that region. Considering (c) and (d), particular features are concerning for module longevity. Features C and D show only minor thermal signatures in the lower reverse injection DLIT image (c). However, in the higher reverse injection DLIT image of the cell, these features show a significant increase in power density. This is because these defects are local sites of reverse bias breakdown (Breitenstein, O., et al, 2011). The measured temperature of these features in the regular thermal image reached over 120 °C. This was in a control climate room of 20 °C. However, in real operation when encapsulated, it is likely that these temperatures could become much higher. Encapsulant material melts within the temperature range of 90 – 120 °C (Crawford, R. and Throne, J., 2002). From this result, it is clear that it is possible that the burn marks found in Figure 1 could have been caused by the reverse biasing of the PV cell, causing severe localised heating.

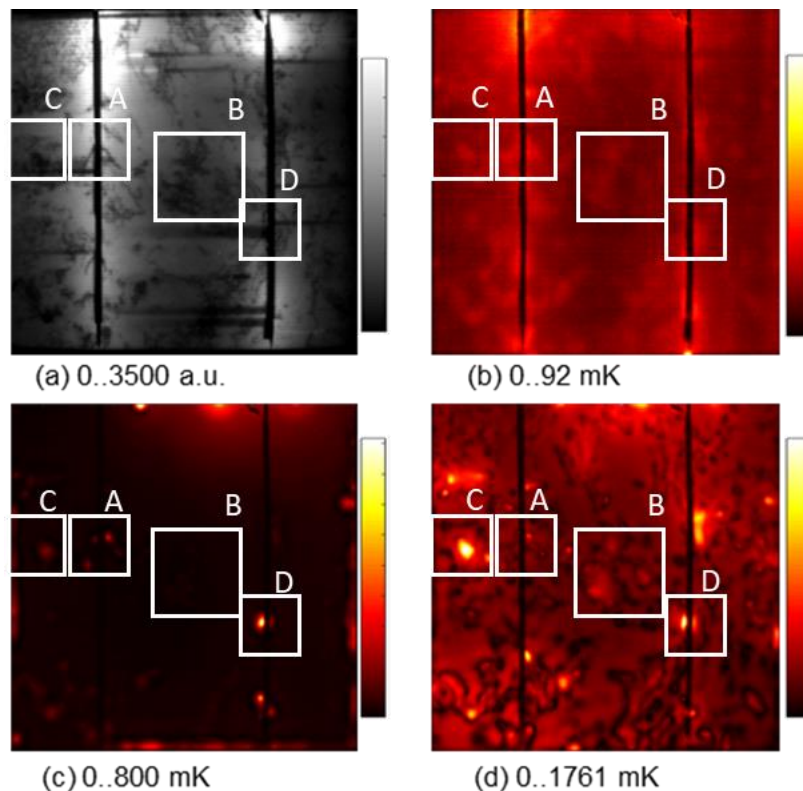


Figure 4 (a) EL of Si PV cell at 10 A and 0.7 V, (b) DLIT 10 A and 0.7 V, (c) DLIT -2A and -18V, (d) DLIT -8 A and -22V.

Out of curiosity, the cell was further reversed biased for an extended period. This caused the cell to crack. To determine the functionality of the PV cell, a DLIT image was acquired at an injection current of 10 A. Figure 5 is the resultant DLIT image. The change in local power density can be seen in the image, indicating a change in the device's electrical properties. While the device still functions, it is likely that its performance has been adversely affected.

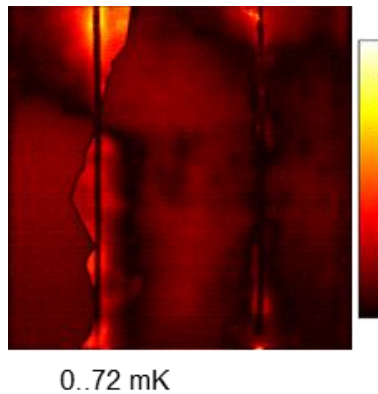


Figure 5 DLIT image of damaged Si PV cell at 10 A and 0.7 V

4. Conclusions and recommendations

Thermo-opto-electrical characterisation has shown to be an effective tool for determining defects within PV devices and electrical characteristics. Thermo-opto-electrical characterisation has also been effectively used to determine a plausible origin of an in-field operational failure of a PV module. More specifically, the burn marks found on the back sheet of an in-field PV module were likely caused by reverse bias-induced localised heating of the PV cell which in turn damaged the encapsulating layer and backsheet. This indicates that it is important for PV power plant maintenance staff to minimise the risk of shading individual cells of operational modules which causes a mismatch. Module cleaning, for example, might not only ensure optimal performance of the module but also improve its longevity.

References

Weaver, J., 2022. *World has installed 1TW of solar capacity*. [online] pv magazine International. Available at: <<https://www.pv-magazine.com/2022/03/15/humans-have-installed-1-terawatt-of-solar-capacity/>> [Accessed 3 October 2022].

Smith, T. 2021. *SA C&I sector starting to make inroads into solar PV market*. [online]. Available at: <<https://www.esi-africa.com/industry-sectors/future-energy/sa-ci-sector-starting-to-make-inroads-into-solar-pv-market/>> [Accessed 28 September 2022].

Haney, J., Burstein, A., 2013. *PV System Operations and Maintenance Fundamentals Solar*, 2013. [Online]. Available at: <http://www.solarabcs.org/O&M>, [Accessed 28 September 2022].

Bauer, J., Breitenstein, O. and Wagner, J., 2009. *Lock-in Thermography: A Versatile Tool for Failure Analysis of Solar Cells*. EDFA Technical Articles, 11(3), pp.6-12.

Fuyuki, T., Kondo, H., Yamazaki, T., Takahashi, Y., and Uraoka, Y., *Photographic surveying of minority carrier diffusion length in polycrystalline silicon solar cells by electroluminescence*, Applied Physics Letters, vol. 86, p. 262108, 2005.

Würfel, P. 2005. *Physics Of Solar Cells – From Principles To New Concept*, Wiley, Weinheim.

Buerhop, C., Pickel, T., Dalsass, M., Scheuerpflug, H., Camus, C., Brabec, C.J., 2016. *aIR-PV-check: A quality inspection of PV-power plants without operation interruption*. In: 43th IEEE Photovoltaic Specialist Conference Proceedings, Portland, Oregon, USA, 1–5, 10.1109/PVSC.2017.8366365.

Dotenco, S., Dalsass, M., Winkler, L., Würzner, T., Brabec, C., Maier, A., Gallwitz, F., 2016. *Automatic detection and analysis of photovoltaic modules in aerial infrared imagery*. In: 2016 IEEE Winter Conference on Applications of Computer Vision (WACV), Lake Placid, NY, USA, Jun. 2016, pp. 1-9, doi:10.1109/WACV.2016.7477658.

Vumbugwa, M., Vorster, F., Crozier McClelland, J. and van Dyk, E., 2022. *Effects of changing partial cell shading on the electrical and thermal characteristics of crystalline silicon photovoltaic module*. Solar Energy.

Vumbugwa, M. 2022, *Investigation of Thermal and Electrical Characteristics of crystalline silicon Photovoltaic modules under varying operational conditions*, Nelson Mandela University, Gqeberha.

Rau, U., 2007. *Reciprocity relation between photovoltaic quantum efficiency and electroluminescent emission of solar cells*. Physical Review B, 76(8).

Fuyuki T, Kitiyanan A. *Photographic diagnosis of crystalline silicon solar cells utilizing electroluminescence*. Appl Phys A. 2008;96(1):189-196.

Dix-Peek, R., van Dyk, E., Vorster, F. 2021. *Maximum power estimation through injection dependent electroluminescence imaging*. Energy Sci Eng. 2021;9:757–767. <https://doi.org/10.1002/ese3.858>

Breitenstein, O., Rakotoniaina, J., Al Rifai, M. and Werner, M. (2004). *Shunt types in crystalline silicon solar cells*. Progress in Photovoltaics: Research and Applications, 12(7), pp.529-538

Breitenstein, O., Bauer, J., Bothe, K., Kwapil, W., Lausch, D., Rau, U., Schmidt, J., Schneemann, M., Schubert, M., Wagner, J. and Warta, W. (2011). *Understanding junction breakdown in multicrystalline solar cells*. J. of Appl. Phys., 109(7), p.071101.

Crawford, R. and Throne, J., 2002. *Rotational molding technology*. Norwich: Plastics Design Library/William Andrew Pub.